TWELFTH EUROPEAN ROTORCRAFT FORUM

Paper No. 29

APPLICATION OF A 3D EULER CODE TO TRANSONIC BLADE TIP FLOW

H. Stahl

Messerschmitt-Bölkow-Blohm GmbH

Munich, F.R. Germany

September 22 - 25, 1986

Garmisch-Partenkirchen

Federal Republic of Germany

Deutsche Gesellschaft für Luft- und Raumfahrt e.V. (DGLR)
Godesberger Allee 70, D-5300 Bonn 2, F.R.G.

APPLICATION OF A 3D EULER CODE TO TRANSONIC BLADE TIP FLOW

H. Stahl
Messerschmitt-Bölkow-Blohm GmbH

Abstract

Due to the 3D unsteady rotational and transonic flow on the advancing blade of a helicopter in fast forward flight, the theoretical analysis on the blade tip is rather complicated.

The application of potential flow theory leads to problems due to the velocity gradient along the blade span because it assumes irrotational flow conditions. The Euler equations do not have this restriction and are therefore more suitable for the calculation of the flow around blade tips.

For the first approach, the 3D steady case will be considered. For the computations, the EUFLEX code (3D steady procedure) developed for flows around fixed wings has been modified for rotor flow conditions. Because of high computation time usually needed for Euler codes a method of step-by-step mesh refinement starting on the coarsest grid has been introduced. In this way computation time can be reduced significantly without loss of accuracy.

It will be shown that there is a strong dependency of the resolution of the grid and the resolution of aerodynamics coefficients. A finer grid supplies better results. Another interesting aspect is the effect of the overall size of the grid. The grid has to be large enough that its outer boundaries can be considered to be in the undisturbed flow so that far field conditions apply.

1. Introduction

During the last years many efforts have been undertaken to optimize the blade tip shape for reducing power consumption, noise and vibrations caused by drag and other transonic effects in fast forward flight. Various tip shapes have been tested in wind tunnels or in flight tests (fig. 1 (1)).

Because of high wind tunnel and flight test costs there is a strong interest in using computational methods for layout of optimal blade tip shapes.

Methods of calculating tip shape effects are numerous and were generally based on potential flow theory. Because this theory is restricted to irrotational flow but the rotor flow is not, there are now efforts undertaken to apply the Euler equations to the blade tip flow (2,3). But Euler codes need much more storage capacities and CPU time than a potential flow code does. By the availability of supercomputers, it has become possible to solve the Euler equations in rather acceptable times and costs.

The computer used for the Euler calculations herein is the Fujitsu VP200 at the IABG in Ottobrunn (Munich). It is available for two years and the needed CPU times are much lower than on a conventional computer, especially, when the used computer code (4) is fully vectorized.

2. Computational Grid

For solving the Euler equations a spacial grid is necessary around the body considered. In this case an H-type grid is used. The outer boundaries of the grid form a cube-like body with plane surfaces where far field conditions are easy to define (see fig. 7).

The grid is generated by an analytical procedure. The most important features are clustering of grid lines in regions where steep gradients of flow variables are expected - that is at the leading edge, trailing edge and near blade tip - and the continuous change of the size of adjacent grid cells.

The last requirement stems from the numerical procedure of the Euler solution. The flow variables are given at the cell center points. But for up-dating the grid cells the values on their surfaces are needed and are determined by a simple averaging the values of the center points (fig. 2). When the grid cells are equally spaced the values achieved are exactly those of the cell surface. Generally, the size of adjacent grid cells is different and the used averaged values are not identical with that of the cell surface. This introduces a numerical error into the computation.

3. Numerical Procedure

For the evaluation of the Euler Equations (EE) and the transformation into curvilinear coordinates of the grid see (4) for detail. Here the numerical procedure will be described.

The basic equations are as follows:

$$\begin{bmatrix} \rho \\ \rho u \\ \rho v \\ \rho w \\ e \end{bmatrix}^{\cdot} + \begin{bmatrix} \rho u \\ p+\rho u^2 \\ \rho uv \\ \rho uw \\ u(\varkappa p+e) \end{bmatrix}_x + \begin{bmatrix} \rho v \\ \rho uv \\ p+\rho v^2 \\ \rho vw \\ v(\varkappa p+e) \end{bmatrix}_y + \begin{bmatrix} \rho w \\ \rho uw \\ \rho vw \\ p+\rho w^2 \\ w(\varkappa p+e) \end{bmatrix}_z = 0$$

where the first term is called flux vector.

Mathematically the EE are solved by the flux-splitting method. It is based on the assumption that the flux vector can be computed separately for each coordinate direction and the solutions can be superimposed.

The EE are numerically solved by means of finite volume method where in the center of each grid cell the flux vector is defined by the flow characteristics ρ, ρu, ρv, ρw, e. The flux vector is to be recalculated at each time step. For the determination of the flux vector the values of cells at the right and the left hand side of the cell considered are required. Missing fluxes of theoretical cells inside of a solid surface have to be extrapolated from known values (fig. 3).

When starting the iteration all values of the grid cells are set to far field conditions. During the first iteration step a flux change appears near the solid surface. This disturbation travels through the following cells to the last grid cell in counting direction (fig. 3). But with each iteration this disturbation moves only one cell against counting direction. From this fact it follows that the higher the number of grid cells in front of the body the more iterations are necessary until the first cell knows from the existance of the body and the more iterations are needed for convergence as well.

The grid refinement procedure used herein is based on this fact. With each grid refinement, in this case done in two steps, the resolution of the grid is doubled and the iteration is restarted with flux vectors that include already the flow disturbations of the foregoing grid.

The most iterations are done on the coarsest grid and the fewest on the finest grid. The values of the flux vectors then are assumed to be the result desired. Convergency control is supplied by the residuum (an average of the maximum differences of the vector of the actual and the foregoing time level) and the lift and drag coefficient, where the drag coefficient shows the lowest convergency speed. The lift coefficient, that is also the pressure coefficient, approaches the end level after rather few iterations. The residuum should approach zero. However, this is not possible because of rounding errors and errors due to discretisation. A typical curve for the residuum is shown in fig. 4.

4. Boundary Conditions

When starting the iteration the flux values of all grid cells are unknown and are to be assumed. Only on the outer boundaries of the grid these values are known and can be prescribed.

It is known that for the incoming flow the density ρ_∞ is constant and the velocity varies along blade radius. The energy of the flow on the grid boundary is to be calculated as function of flow properties. Outboard the blade tip the velocity distribution is unknown and proper assumptions are necessary. Their influences on the numerical solution of the Euler equations are investigated here, too. Two possibilities of velocity distributions are considered (fig. 5):

- the velocity gradient is constant along radius and continues outboard the tip,
- the velocity gradient is constant along radius but changes slope outboard the tip.

5. Results

In the following the computational results achieved by the EUFLEX-Code (4) are shown as function of several grids and different far field conditions.

Throughout these investigations the same geometry of the blade tip (fig. 6) and the same Mach number distribution along blade span ($M_T = 0.8$) is assumed.

The blade tip part considered includes the outer 20 percent of the blade radius with DM-H3 profile at the tip and DM-H4 profile at 0.8 radius. The blade tip speed is 220 m/s, blade radius 5 m, chord 0.27 m, twist - 2°/m radius, and the advance ratio shall be 0.25. Although for these conditions the actual flow is unsteady, it is approximated by a steady solution at $\Psi = 90°$. The basic grid used here has outer grid boundaries a follows:

x - direction: 4 chords upstream
5 chords downstream

y - direction: 3 span outboard

z - direction: 4 chords above
4 chords below

The effect of successive grid refinement is shown in fig. 7 to 9. The resolution of the grids used are given by (fig. 7):

	i x j x k	grid points	iterations
1. grid	20 x 13 x 10	2600	1800
2. grid	39 x 25 x 18	17550	1000
3. grid	77 x 48 x 34	125664	600

When comparing the pressure distributions of the 1. and 2. grid (fig. 8) at the same location, a small increase of the suction peak can be seen on the 2. grid. On the 3. grid, the shape of the pressure distribution is much more realistic than on the coarser grids. It can be concluded that the finer the grid and the higher the resolution of the surface (especially in regions of steep curvature of the surface) the more accurate the solution.
Fig. 9 shows the effect of grid refinement on the lift and drag coefficient.

The effect of attracting the grid lines to the surface is shown in fig. 10 to 12. The grids have the same dimensions as the 3. grid above. The attraction of the grid lines to the body surface is done by means of an exponential function a^n, a describing the relation of the distance of the grid point to the surface normalized by the distance of the grid outer surface to the body surface, and n = 1.2 and 2.0 (fig. 10).

The difference of the results can be seen at the pressure distribution (fig. 11) as well as at the lines of constant Mach number on the blade surface (fig. 12). Especially on the upper side there are large differences in the leading edge region up to about 25 % chord downstream. When the grid lines are closer to the surface the suction peak is closer to the leading edge and the pressure distribution is more concentrated in the leading edge region.

For getting an Euler solution as accurate as possible a very high resolution of the body surface is required. This means a large number of cells and high CPU-times. When using a grid refinement procedure like here the CPU-time decreases appreciately without loss of accuracy. But the high resolution of the body surface alone is not sufficient. Because the flux values are calculated at the center point of the grid cell they are not the values immediately at the surface but a small distance away. The gradients of the flow close to the surface are much steeper than in the flow field farther away, and in this way a stronger attraction of grid lines to the body surface (that means the height of the grid cell) also influences the numerical solution.

The effect of the dimension of the grid is shown in fig. 13 to 15. For this investigation the number of grid points and the number of points on the blade surface and their distribution are the same as on the 3. grid above. Only the dimensions of the grid are different (fig. 13). The original grid shall be called "large" grid (A) and the other one "small" grid (B) which is given by:

small grid (B)

x-direction:	one chord upstream
	one chord downstream
y-direction:	1.5 span outboard
z-direction:	one chord above
	one chord below

From fig. 14 it can be seen that the pressure coefficient on the small grid has much a higher suction peak at the leading edge especially on the lower side. But this is not an indication of a too small grid. This conclusion may follow from the plot of ISO-Mach lines (fig. 15). On the large grid the Mach lines spread out smoothly into the far field. On the small grid the outer Mach lines follow the outer grid boundaries. That might serve as a criterion.

When the grid dimensions are too small it cannot be assumed that the disturbations due to the body are sufficiently decayed up to the grid boundaries, and the far field conditions are not valid there.

The effect of the boundary conditions is shown in fig. 16 and 17. Two different velocity distributions outboard the blade tip are compared (fig. 5).

For this investigation grid and velocity distribution along blade radius are unchanged. The differences of the pressure distributions shown in fig. 16 are rather small. On the ISO Mach number plots (fig. 17) some differences can be observed on the upper side in the leading edge region up to about 25 % chord. Also the supersonic region of M = 1.02 of case A is a little more extended than in case B.

Lowering the velocity distribution outboard the tip causes a slight lowering of the overall level of the pressure distribution. Fig. 18 shows this effect very drastically for a pressure distribution on a coarser grid. Here the velocity level outboard the tip is very low as shown in fig. 19.

Conclusion

For the flow around a rotating blade results of a steady state solution of the Euler equations are shown for an advancing blade at $\Psi = 90°$. Investigations are performed on a certain geometric configuration to determine the influences of grid and boundary conditions.

From the investigation of the grid parameter it can be concluded that

- the resolution of the body surface has to be as high as possible especially in regions with steep curvatures and regions where steep flow gradients are expected;
- attracting the grid lines to the body surface gives better results because the cell center points are closer to the body surface and in this way the flow values are closer to those at the surface itself;
- the grid boundaries have to be so far away from the body that disturbations due to the body can be assumed to have sufficiently decayed and far field conditions apply.

From the investigation of different velocity distributions outboard the tip follows that a decaying velocity outboard the tip lowers the overall level of the pressure distribution on the blade. For further investigations, comparisons with measurements are necessary for controlling numerical solutions.

Literature

1. D.T. Balch — Impact of main rotor tip geometry on main rotor/tail rotor interaction in hover
40th annual forum of AHS, Alexandria, Virginia, May 1984

2. R.K. Agarwal, J.E. Deese — Euler calculation for the flow field of a helicopter rotor in hover
AIAA-86-1782-CP

3. T.W. Roberts, E.M. Murman — Euler solutions for the flow around a hovering rotor
AIAA-86-1784-CP

4. A. Eberle — A new flux extrapolation scheme solving the Euler equations for arbitrary 3-D geometry and speed, MBB-EUFLEX
MBB/LKE122/S/PUB/140, 1984

5. H. Stahl — The problem of calculation of the flow around helicopter rotor blade tips
7th European Rotorcraft and Powered Lift Aircraft Forum, Garmisch-Partenkirchen, Germany, 1981

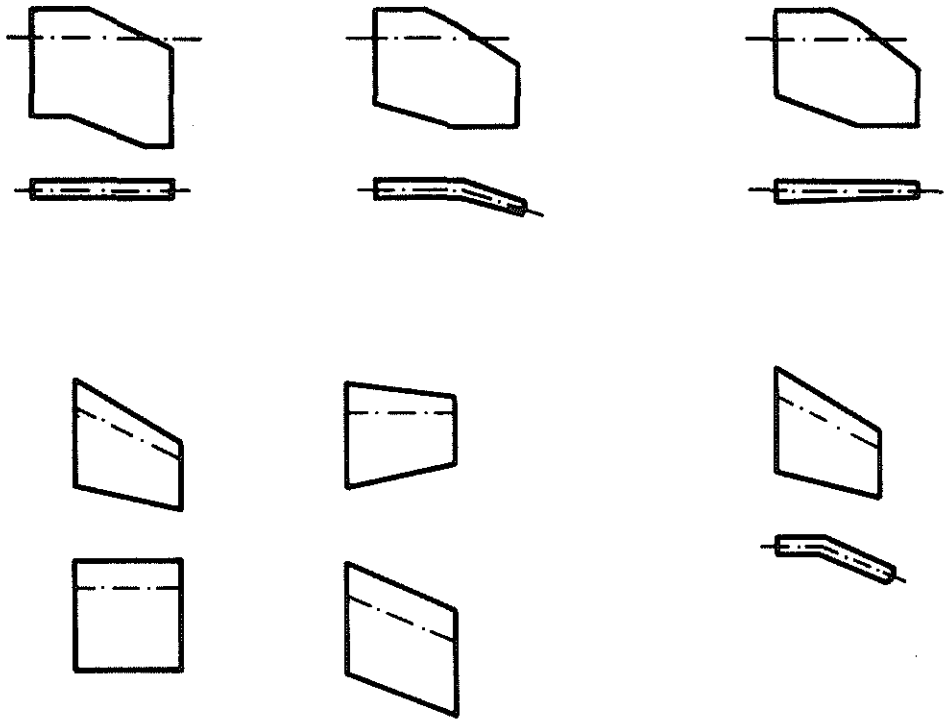

Fig. 1 Example of tested tip shapes

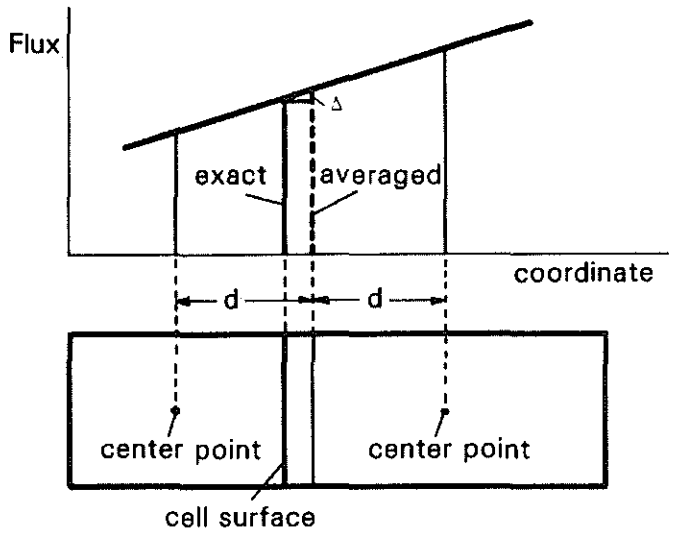

Fig. 2 Determination of flux values at cell surfaces

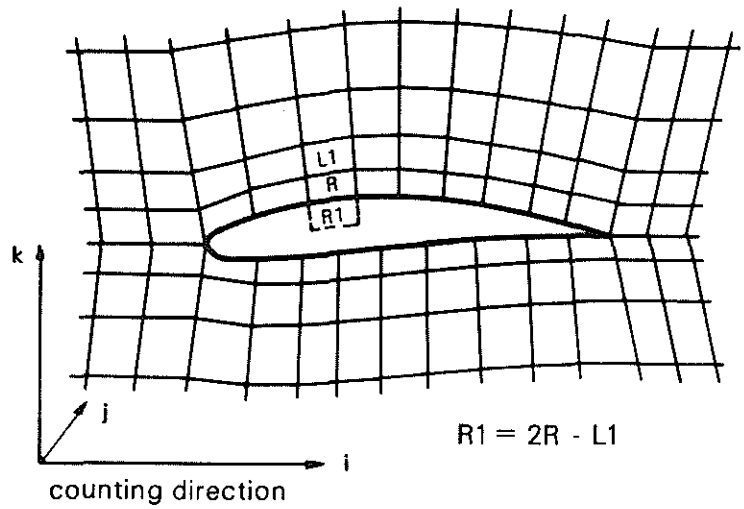

Fig. 3 Flux extrapolation at solid surfaces

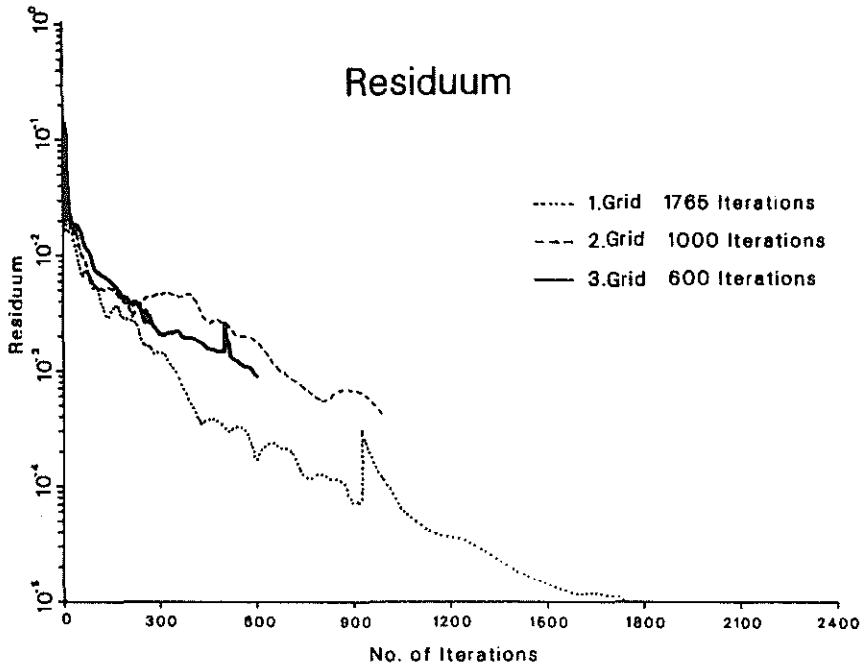

Fig. 4 A typical curve of a residuum

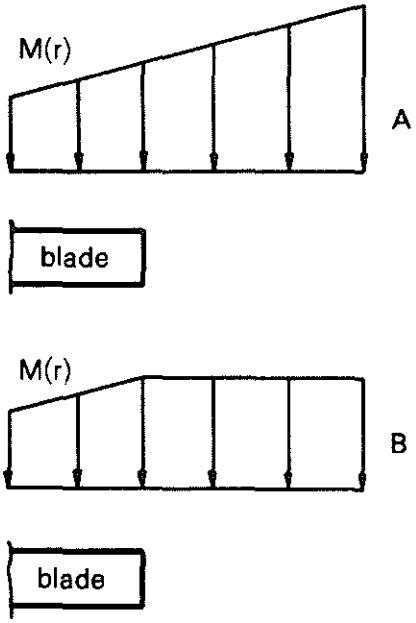

Fig. 5 Two velocity distributions outboard blade tip

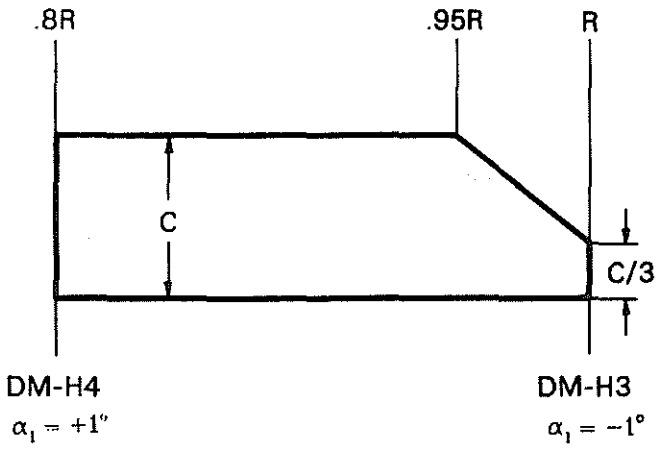

Fig. 6 Geometry of calculated blade tip

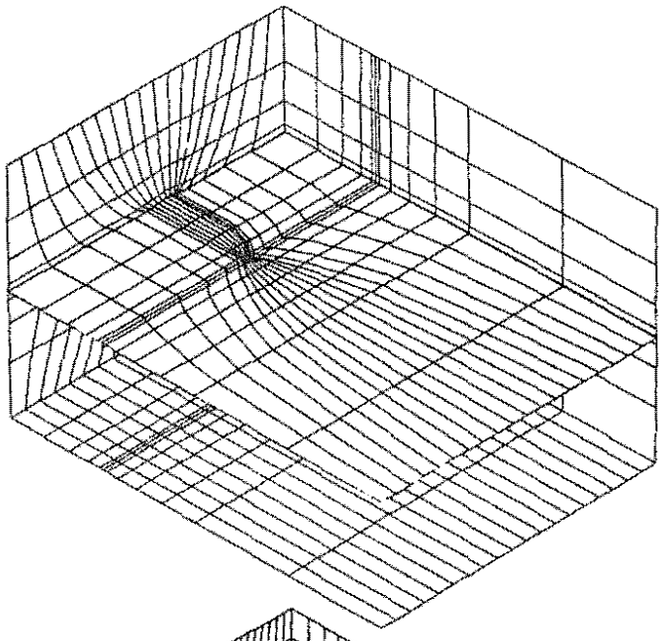

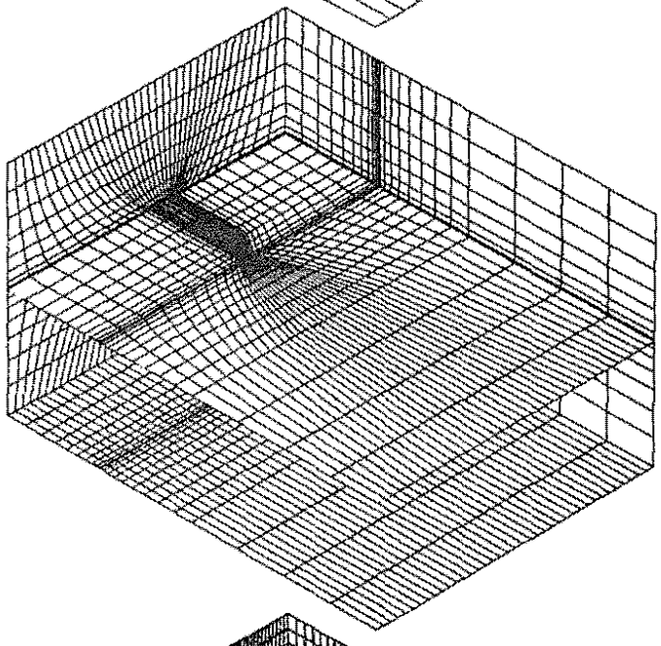

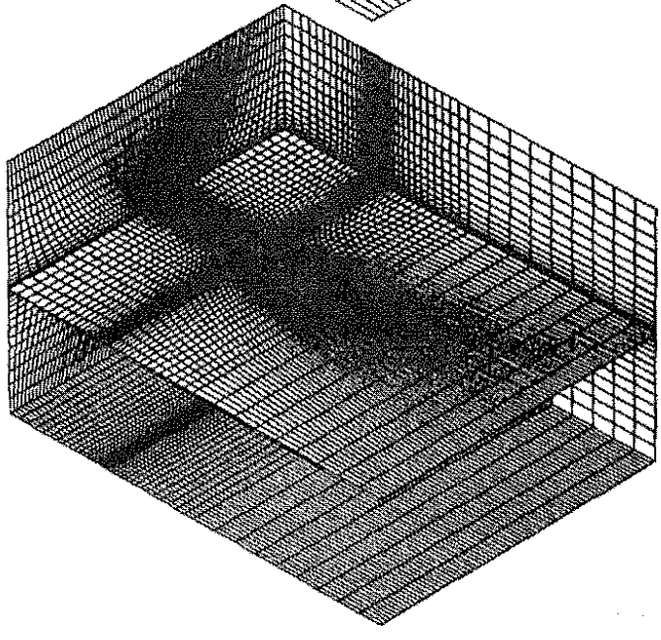

Fig. 7 The 3 steps of grid refinement

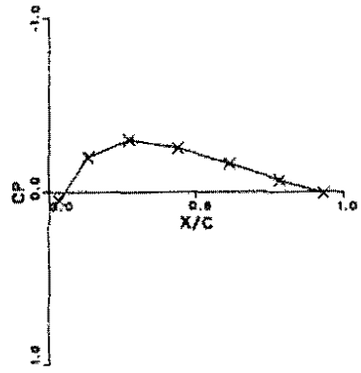

1.Grid

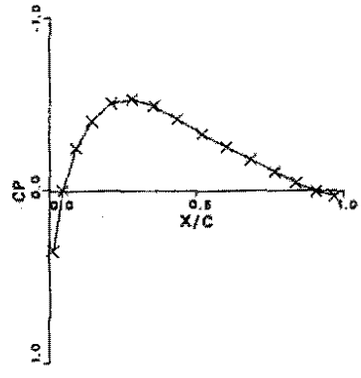

2.Grid

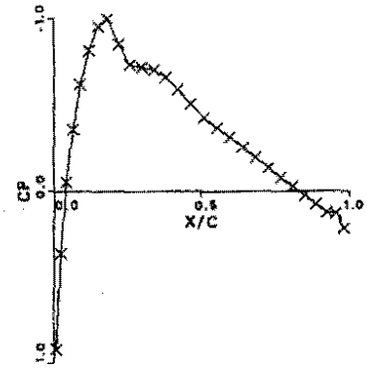

3.Grid

Fig. 8 Pressure distribution at r/R = 0.83

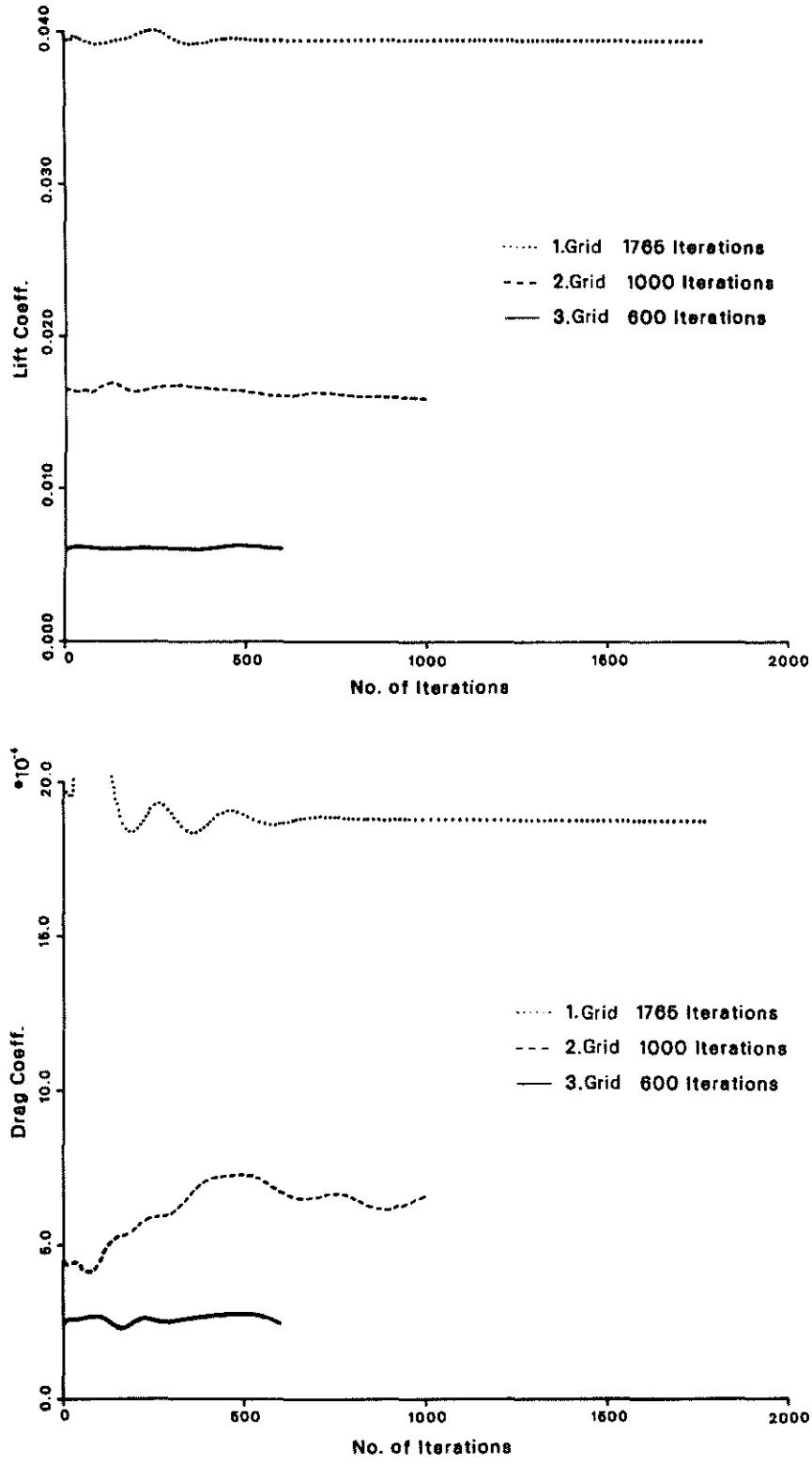

Fig. 9 Effect of grid refinement on local lift and drag coefficient

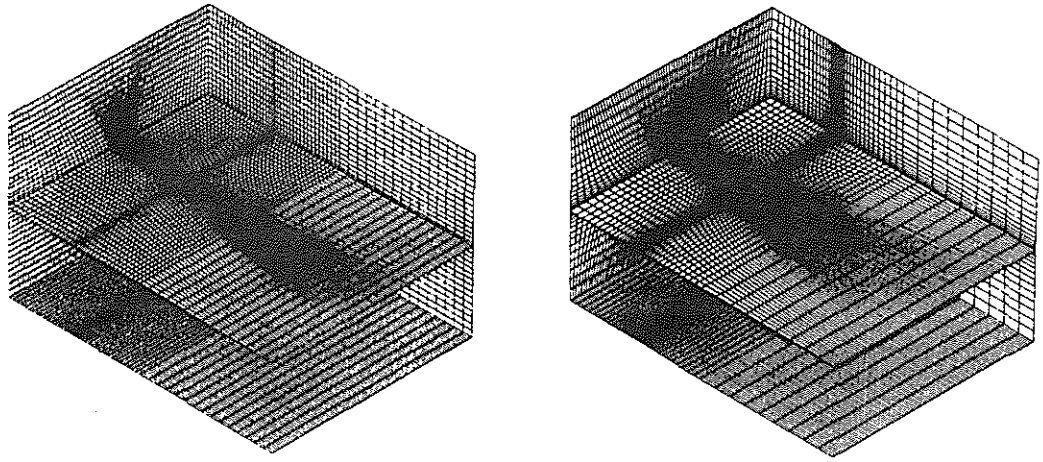

n = 1.2 n = 2.0

Fig. 10 Grid generated by different attraction exponents

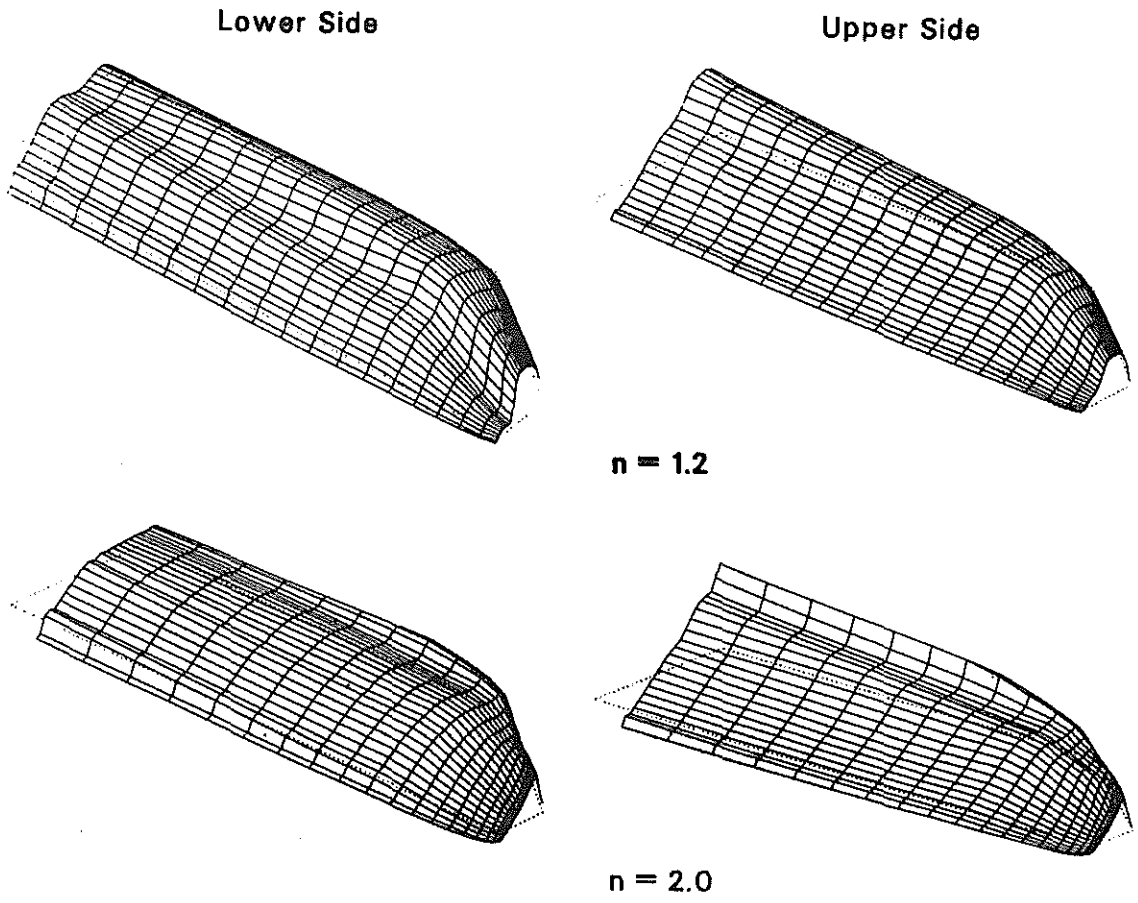

Fig. 11 Effect of clustering grid lines onto pressure distribution

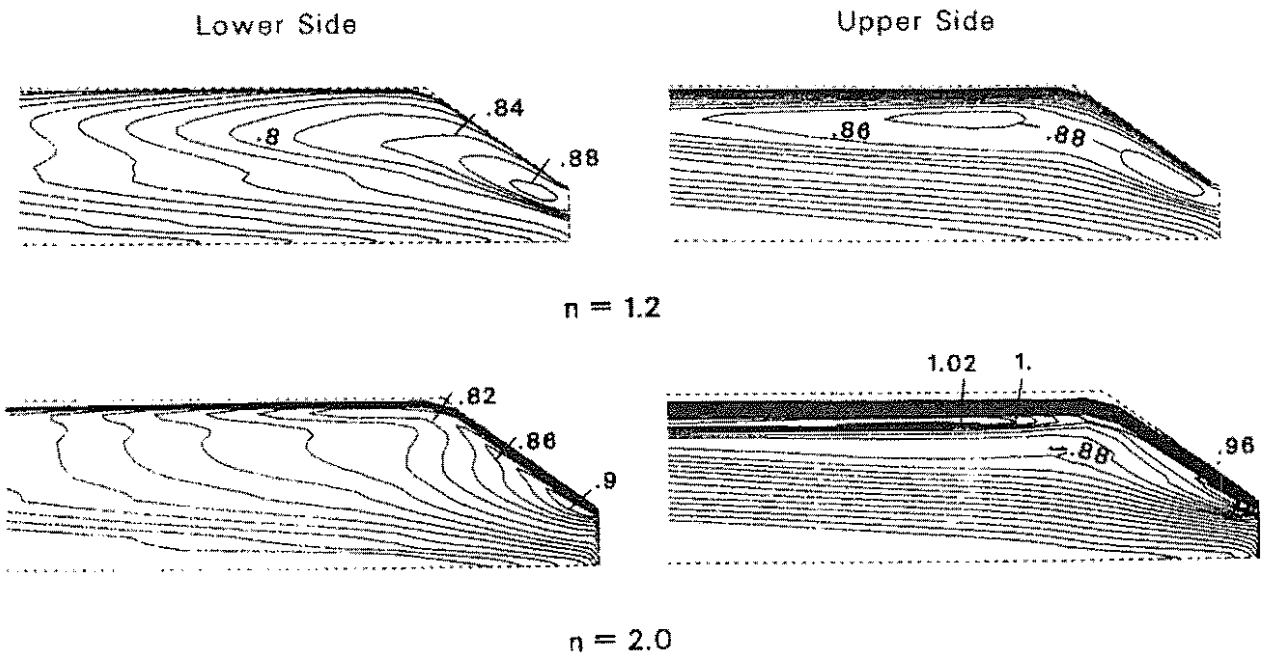

Fig. 12 Effect of clustering grid lines onto lines of equal Mach number

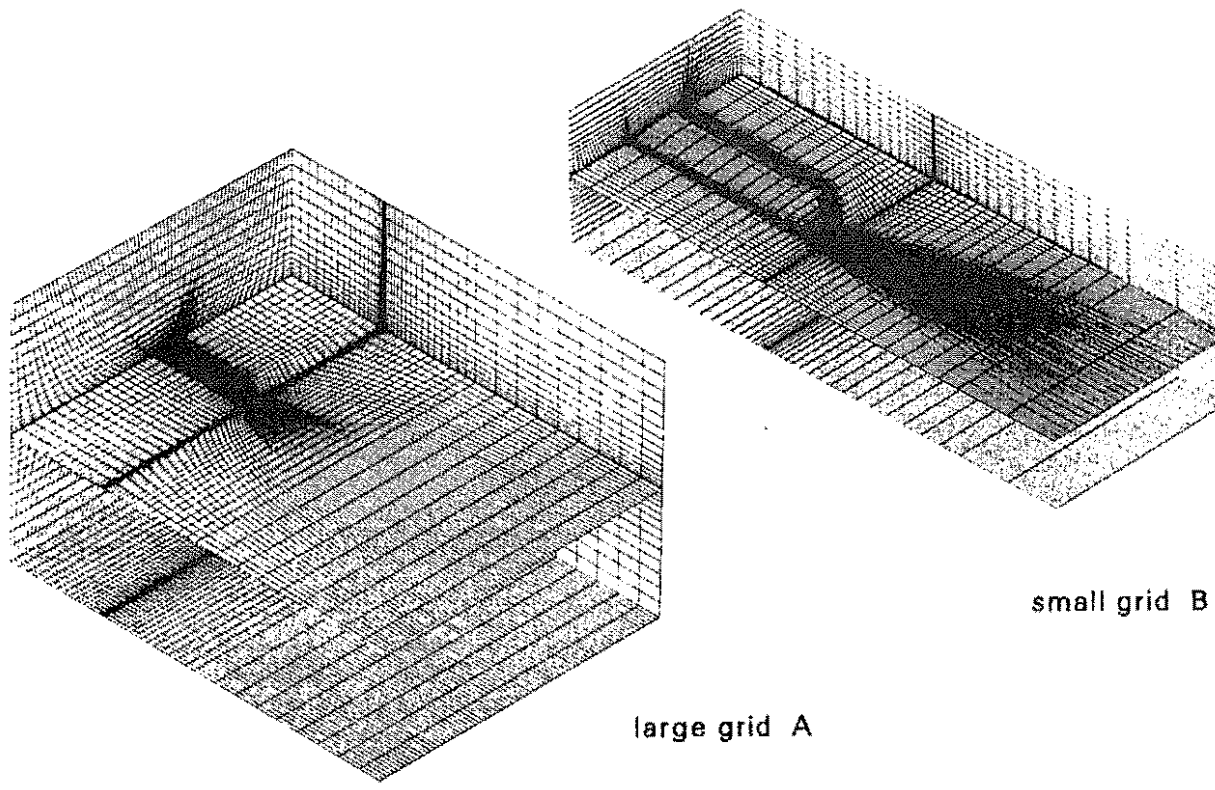

Fig. 13 Grids with different dimensions

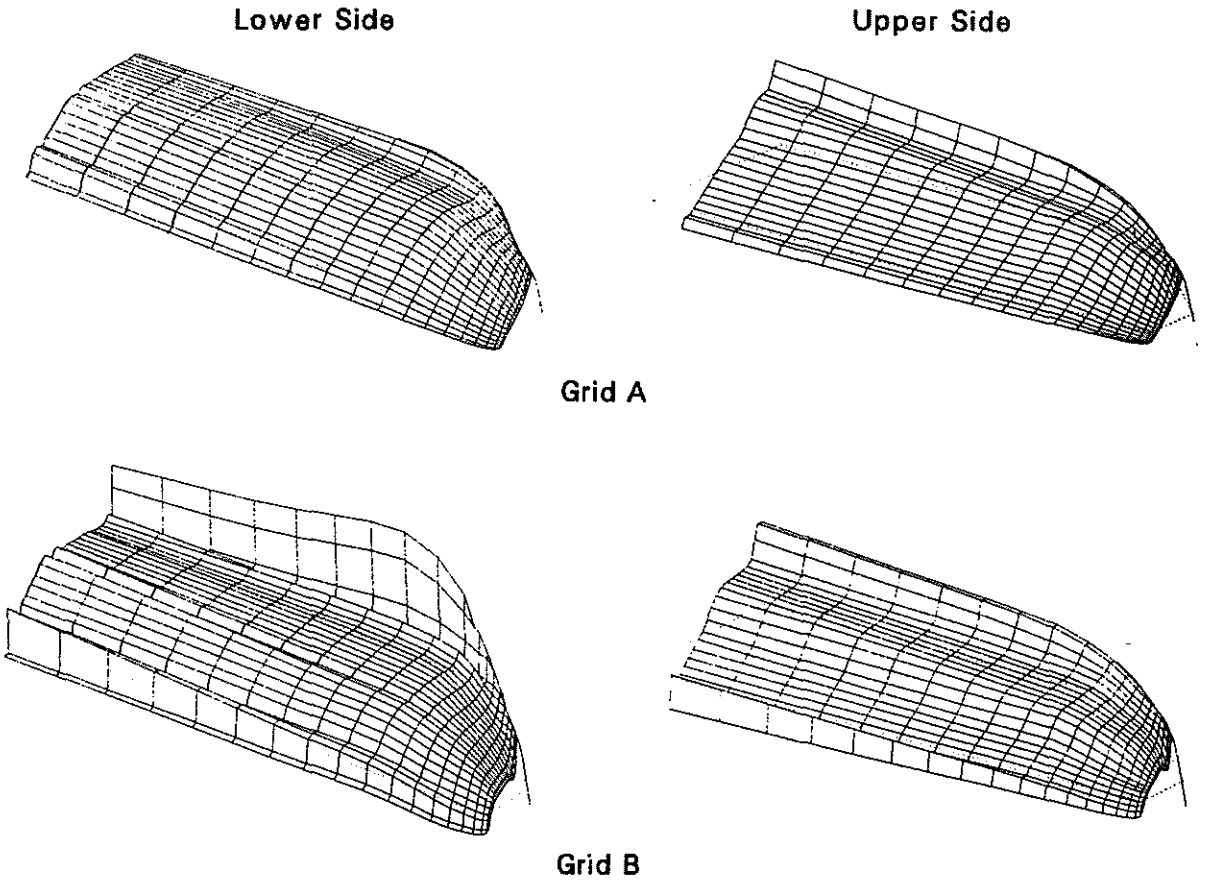

Fig. 14 Pressure distributions for grids with different dimensions

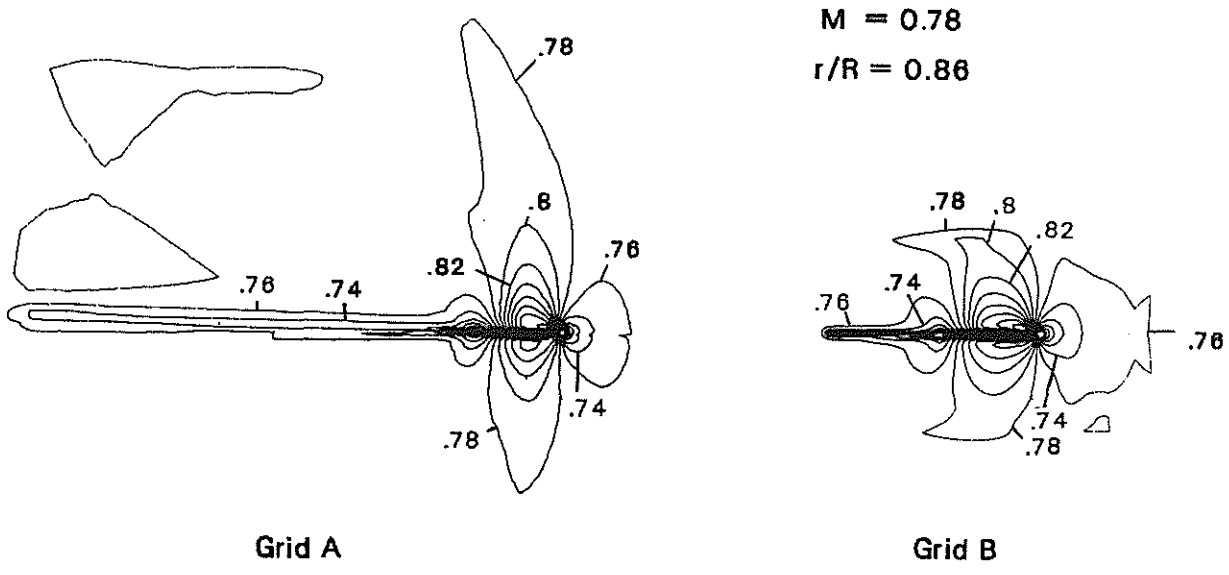

Fig. 15 Effect of grid dimension on lines of equal Mach number

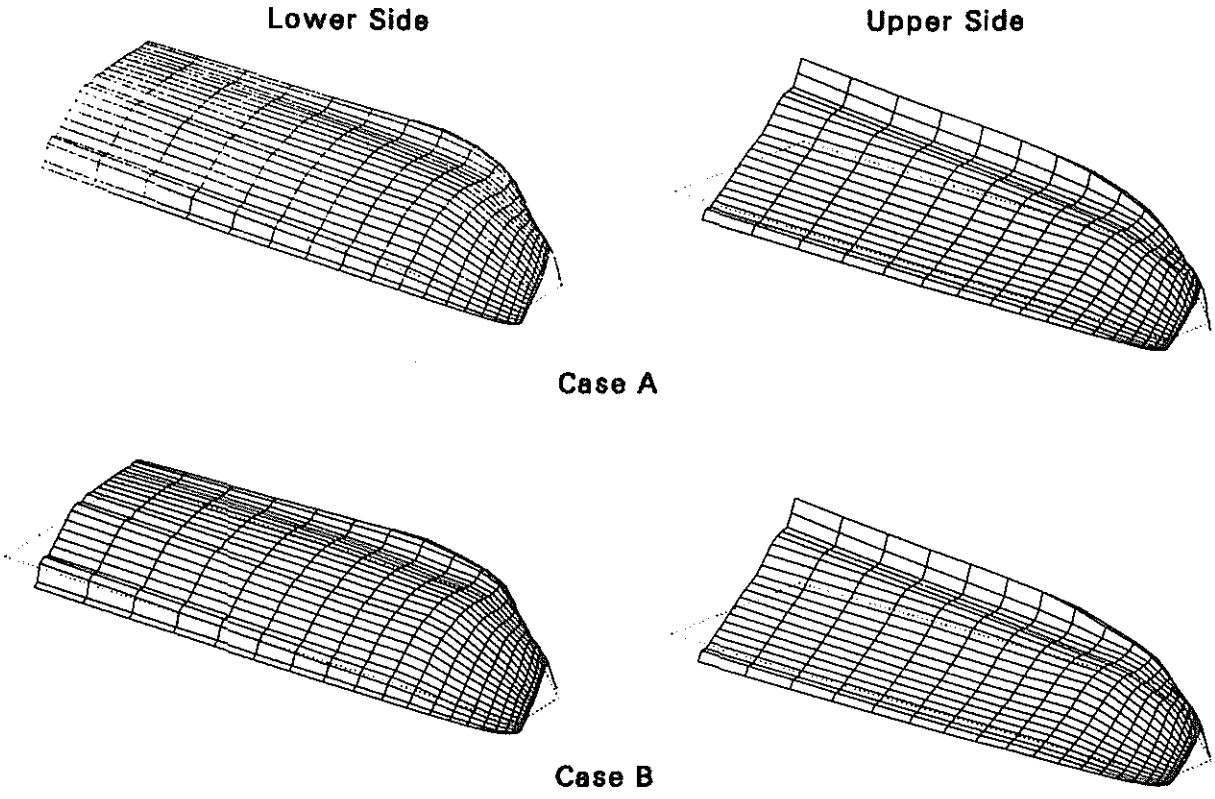

Fig. 16 Effect of the boundary condition on pressure distribution

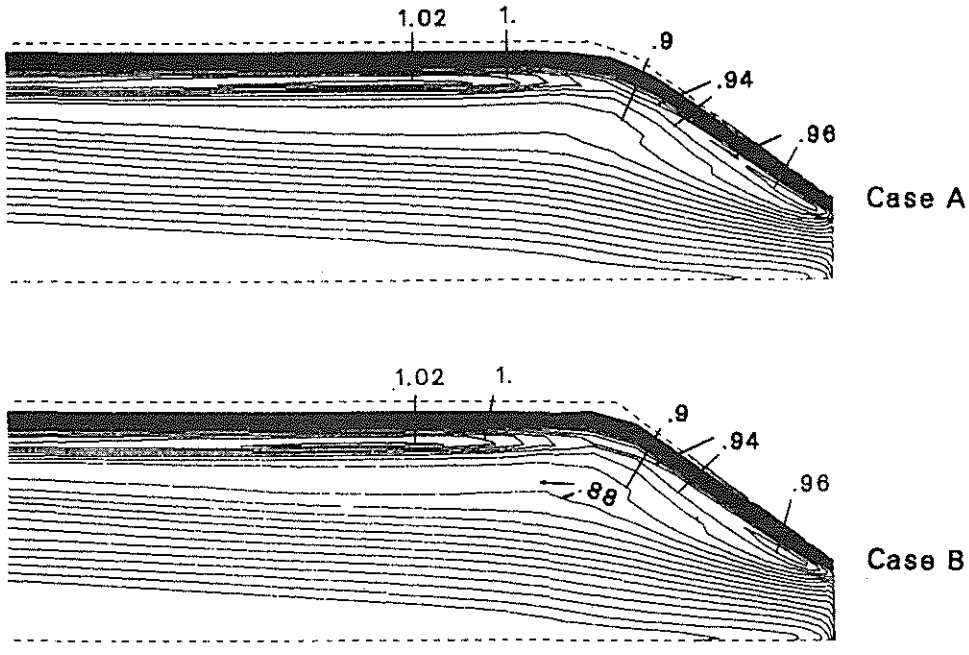

Fig. 17 Effect of the boundary condition on lines of equal Mach number

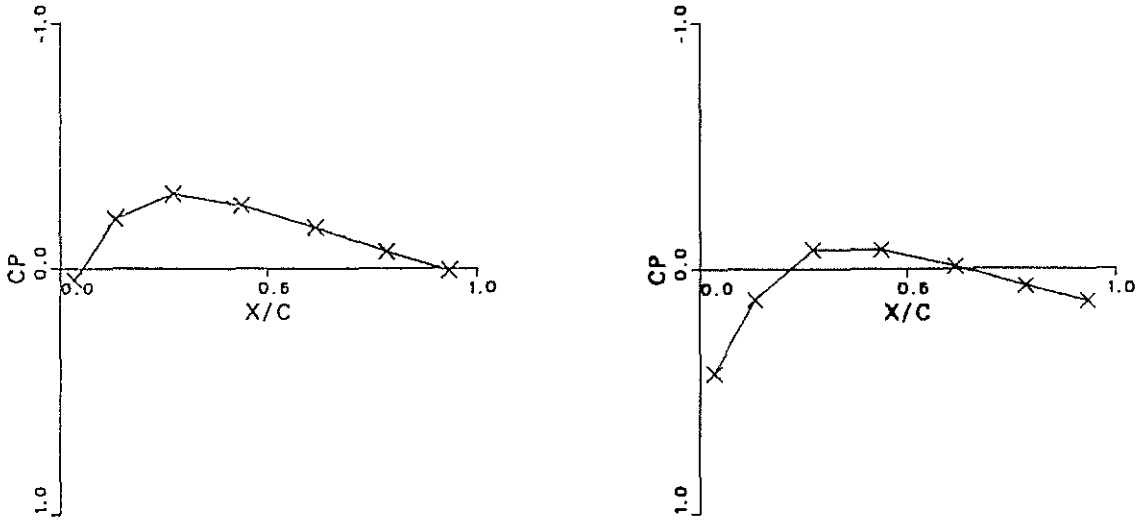

Fig. 18 Pressure distribution at r/R = 0.83

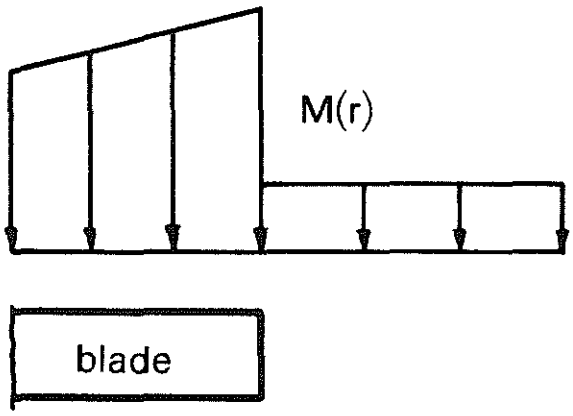

Fig. 19 Velocity distribution with $M_T = 0.8$ and outboard $M = 0.2$